Progress In Electromagnetics Research, Vol. 143, 207–221, 2013

SINGLE-FEED TRIPLE BAND CIRCULARLY POLARIZED SPIDRON FRACTAL SLOT ANTENNA

Thuy Nguyen Thi, Son Trinh-Van, Gina Kwon, and Keum Cheol Hwang*

Division of Electronics and Electrical Engineering, Dongguk University-Seoul, 26, Pil-dong 3-ga, Chung-gu, Seoul 100-715, South Korea

Abstract—In this paper, the design of a single-feed triple-band circularly polarized Spidron fractal slot antenna is presented. The proposed antenna is composed of a Spidron fractal slot, a Z-shaped slit, and two L-shaped slits to realize triple-band circular polarization operation. A simple 50 Ω microstrip line is utilized to feed the proposed antenna. A conducting reflector is also used to reduce back radiation, thereby enhancing the forward antenna gain. The proposed antenna has total dimensions of 40.7 mm × 40.7 mm × 18.52 mm ($0.42\lambda \times 0.42\lambda \times 0.19\lambda$) and was fabricated and tested. The experimental results show that the proposed antenna has −10 dB reflection coefficient bandwidths from 2.76 GHz to 3.13 GHz and from 3.56 GHz to 6.22 GHz. The measured 3 dB axial ratio bandwidths are 2.28% (3.04–3.11 GHz) for the lower band, 7.15% (4.18–4.49 GHz) for the middle band, and 2.6% (4.93–5.06 GHz) for the upper band. The peak gains within the −10 dB reflection coefficient bandwidths are 3.41 dBic and 6.29 dBic, respectively.

1. INTRODUCTION

Circularly polarized (CP) antennas have been widely used in wireless communication systems because of their ability to mitigate propagation effects, reduce polarization mismatch, and enlarge system capability [1–11]. The rapid growth of modern wireless systems has also increased the demand for compact antennas with multi-band resonance. With advantages such as low profile, light weight, and ease of integration with active devices, microstrip antennas

Received 5 September 2013, Accepted 16 October 2013, Scheduled 1 November 2013

* Corresponding author: Keum Cheol Hwang (kchwang@dongguk.edu).

have been a suitable choice for many multi-band CP applications. Various types of microstrip antennas for dual band CP operation have been reported [12–15]. However, CP antennas designed with triple-band operation have attracted very little attention compared to the dual band CP antennas. Recently, several CP antennas employing various techniques to realize triple-band CP operation have been presented [16–21]. In [16–18], the proposed triple-band CP antennas utilized the concept of stacked patches fed by a coaxial probe. A multi-layered Giuseppe Peano fractal antenna with an electromagnetic coupled microstrip feeder was proposed to realize triple-band CP operation in [19]. Although, in general, multi-layered antenna structures make it easier to achieve multi-band CP operation than others, their fabrication is very complex. In order to mitigate these fabrication difficulties, triple-band CP antennas with a single dielectric substrate have been studied. A single-layer triple-band CP antenna which integrated two nonconcentric annular slots and an inverted h-shaped microstrip feed line was proposed in [20]. A maximum 3 dB axial ratio (AR) bandwidth of 85 MHz was achieved in the middle band. In another study, a single-layer triple-band CP antenna design using two pairs of L-shaped slits was investigated [21], but the 3 dB AR bandwidths were no more than 2 MHz. These antennas do have simple structures, but the 3 dB AR bandwidths are relatively narrow. Therefore, designing triple-band CP antennas with improved AR bandwidth continues to be engineering challenge.

In this paper, we propose a CP Spidron fractal slot antenna with a single microstrip feed for triple-band applications. Other examples of fractal antennas for ultra-wideband applications can be found in [22, 23]. The antenna structure is composed of a 50 Ω microstrip line, a conducting reflector, and a substrate, which includes a Spidron fractal slot, a Z-shaped slit, and two L-shaped slits to achieve the triple-band CP operation. The proposed antenna was optimized, fabricated and tested. Sections 2 and 3 describe the detailed antenna configuration and parametric study for major variables, respectively. Section 4 presents the experimental results and discussion; finally, concluding remarks are summarized in Section 5.

2. ANTENNA GEOMETRY

Figure 1 illustrates the geometry of the proposed triple-band CP Spidron fractal slot antenna. The antenna structure is composed of a dielectric substrate, a 50 Ω microstrip feeding line, a ground plane, and a conducting reflector. The antenna is designed on a Taconic RF-35 substrate with a relative dielectric constant of 3.5, thickness of

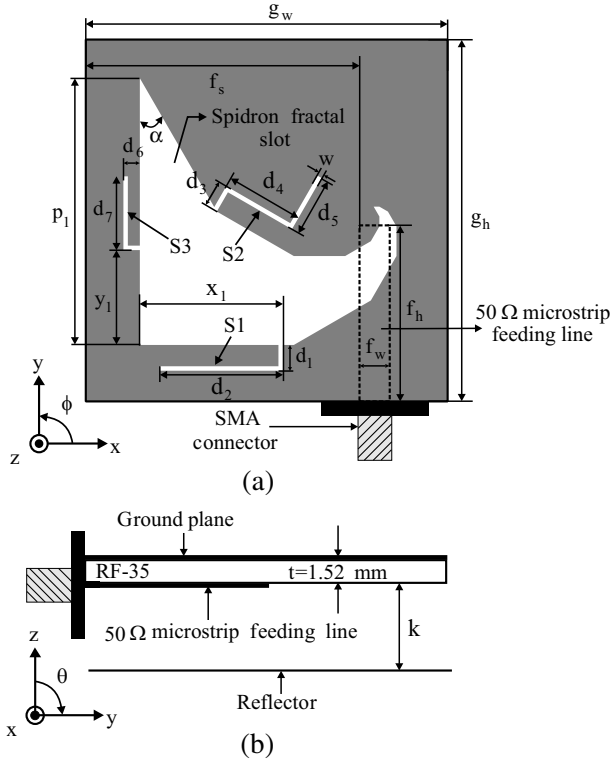

Figure 1. Geometry of the proposed antenna with coordinate system: (a) top view and (b) side view.

1.52 mm, and loss tangent of 0.0018. The triple-band CP operation can be realized by utilizing a Spidron fractal slot, a Z-shaped slit, and two L-shaped slits, which are etched from the ground plane. One of the present authors previously proposed a Spidron fractal slot antenna with single band CP operation [24, 25]. In this work, a Spidron fractal system is formed from a series of contiguous right-angled triangles with identical angular factor (α). The hypotenuse of each right-angled triangle coincides with the adjacent side of a smaller, down-scaled right-angled triangle. This Spidron fractal system is repeated with seven iterations in this antenna design. The parameters of the first right-angled triangle include angle α and its adjacent side with a length of p_1. The scale factor (δ) of the Spidron fractal system is given as follows:

$$\delta = \tan\alpha, \quad \text{for} \quad 0^\circ < \alpha < 45^\circ. \tag{1}$$

Based on previous research on the Spidron fractal antenna, a single band Spidron fractal slot is designed to obtain CP radiation at 4.2 GHz. Then three slits, including two L-shaped slits $S1$ and $S3$, and a Z-shaped slit $S2$, are inserted at the edges of the Spidron fractal slot to generate two additional CP modes (at 3.1 GHz and 5.0 GHz) near the basic CP mode of the Spidron fractal slot. First, CP radiation at 3.1 GHz is obtained by employing slits $S1$ and $S2$. The L-shaped slit $S1$ consists of two rectangular slits with lengths of d_1 and d_2 and is formed at the opposite side of the first right-angled triangle at a distance of x_1 from the left edge of the Spidron fractal slot. The Z-shaped slit $S2$ includes three rectangular slits with lengths of d_3, d_4, and d_5. It is formed at a vertex of the second right-angled triangle of the Spidron fractal slot. The total length of the two slits $S1$ and $S2$ is approximately equal to a half of the guided wavelength at the frequency of 3.1 GHz and is calculated as follows:

$$L_{S1+S2} = \sum_{i=1}^{5} d_i - 3w, \tag{2}$$

where w is the width of all slits. Meanwhile, the CP radiation at 5.0 GHz is mainly induced from slit $S3$. The L-shaped slit $S3$ consists of two rectangular slits with lengths of d_6 and d_7. It is connected to the adjacent side of the angle α at a distance of y_1 from the lower edge of the Spidron fractal slot. The length of slit $S3$ is equal to a quarter of the guided wavelength at the frequency of 5.0 GHz and is calculated as follows:

$$L_{S3} = d_6 + d_7 - w. \tag{3}$$

A 50 Ω microstrip feeding line with the dimensions $f_w \times f_h$ on the bottom layer of the substrate is located at a distance f_s from the left edge of the antenna. To enhance the antenna gain, a conducting reflector is also utilized and placed at a distance k under the substrate. The overall dimensions of the proposed antenna are $g_w \times g_h \times (k + t)$.

3. PARAMETRIC STUDY

The design procedure of the proposed antenna includes three steps for implementing the triple-band CP operation. First, the CP radiation at 4.2 GHz is derived by employing the Spidron fractal slot. Two slits $S1$ and $S2$ are then employed to generate the CP radiation at the lower resonant frequency (3.1 GHz). Finally, an additional CP operation is achieved at the upper resonant frequency of 5.0 GHz by inserting the slit $S3$. Simulation and optimization of the proposed antenna were

conducted by using Ansys High-Frequency Structure Simulator (HFSS) based on the three-dimensional finite element method (FEM) [26].

Figure 2 shows the simulated reflection coefficient and AR of the proposed antenna for three cases: the Spidron fractal slot alone, the Spidron fractal slot with slits $S1$ and $S2$, and the Spidron fractal slot with three slits $S1$, $S2$, and $S3$. It is clearly seen that the proposed antenna with the single Spidron fractal slot exhibits CP operation in the middle band (4.2 GHz). Meanwhile, as shown in the figure, utilizing slits $S1$ and $S2$ generates CP radiation in the lower band (3.1 GHz), and another slit $S3$ adds the additional CP operation in the upper band (5.0 GHz). The effect of the total length of slits $S1$ and $S2$ (L_{S1+S2}) on the reflection coefficient and AR is shown in Fig. 3. It is observed that L_{S1+S2} affects CP operation in the lower band, whereas it does not have much effect on CP operation in either the middle band or upper band. The resonant frequency and operating CP frequency, where the minimum AR exists, both decrease as length L_{S1+S2} increases. Fig. 4 illustrates the influence of length L_{S3} on the reflection coefficient and AR. Like the result shown in Fig. 3, the length of slit $S3$ only affects CP operation in the upper band. The operating CP frequency in the upper band is shifted up to a higher band as

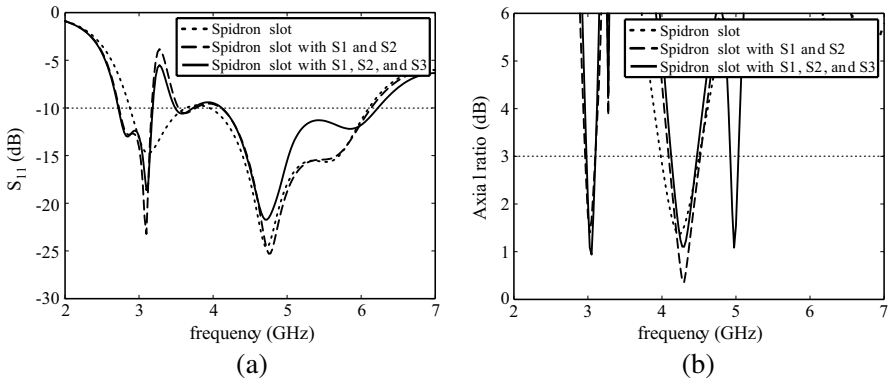

Figure 2. Simulated results of (a) reflection coefficient and (b) axial ratio of the proposed antenna for three cases: the Spidron fractal slot alone, the Spidron fractal slot with slits $S1$ and $S2$, and the Spidron fractal slot with three slits $S1$, $S2$, and $S3$ when $p_1 = 30\,\text{mm}$, $\alpha = 30^\circ$, $g_w = 40.7\,\text{mm}$, $g_h = 40.7\,\text{mm}$, $k = 17\,\text{mm}$, $f_h = 19.8\,\text{mm}$, $f_w = 3.4\,\text{mm}$, $f_s = 30.7\,\text{mm}$, $x_1 = 16.09\,\text{mm}$, $y_1 = 10.67\,\text{mm}$, $d_1 = 2.9\,\text{mm}$, $d_2 = 13.84\,\text{mm}$, $d_3 = 3\,\text{mm}$, $d_4 = 8.8\,\text{mm}$, $d_5 = 6.65\,\text{mm}$, $d_6 = 1.85\,\text{mm}$, $d_7 = 8.3\,\text{mm}$, $w = 0.5\,\text{mm}$, $L_{S1+S2} = 33.69\,\text{mm}$, and $L_{S3} = 9.65\,\text{mm}$.

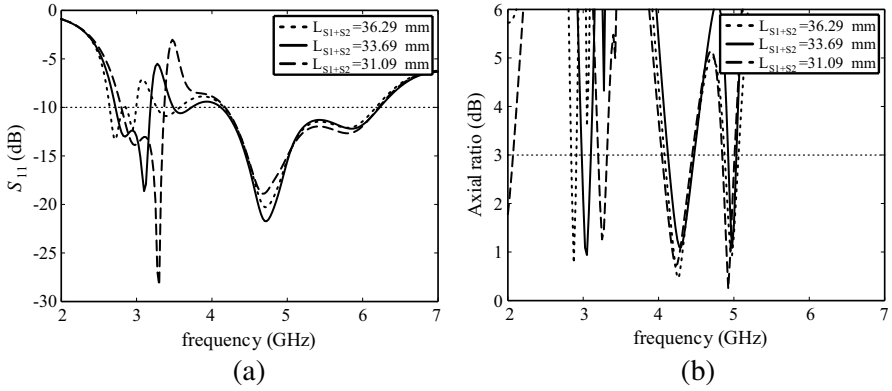

Figure 3. Simulated results of (a) reflection coefficient and (b) axial ratio with different values of L_{S1+S2}.

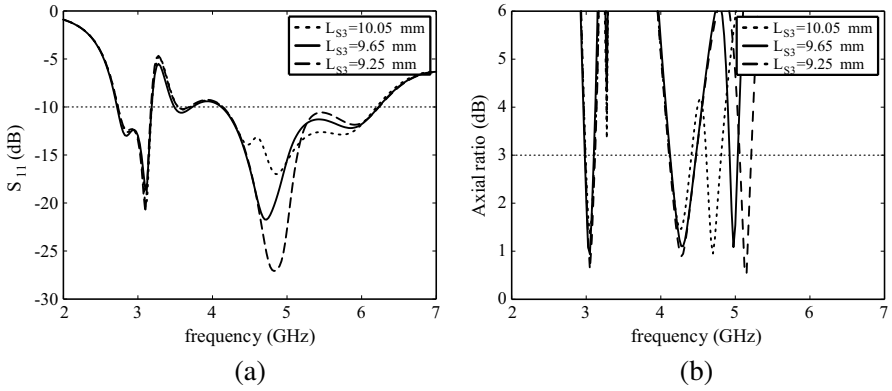

Figure 4. Simulated results of (a) reflection coefficient and (b) axial ratio with different values of L_{S3}.

the length L_{S3} decreases, without deteriorating the CP performance in the lower band and middle band. Therefore, the CP performance of the proposed antenna can be independently tuned at three different frequencies by the Spidron fractal slot and three slits engraved on each side.

We also simulated magnetic current concentrations on the aperture to visualize the CP operation of the antenna. Fig. 5 depicts the current distribution, as observed from the $+z$-direction at 3.1 GHz. Here, Mtotal represents the vector sum of all major current contributions. At $t = 0$, the currents on slits $S1$ and $S2$ and the

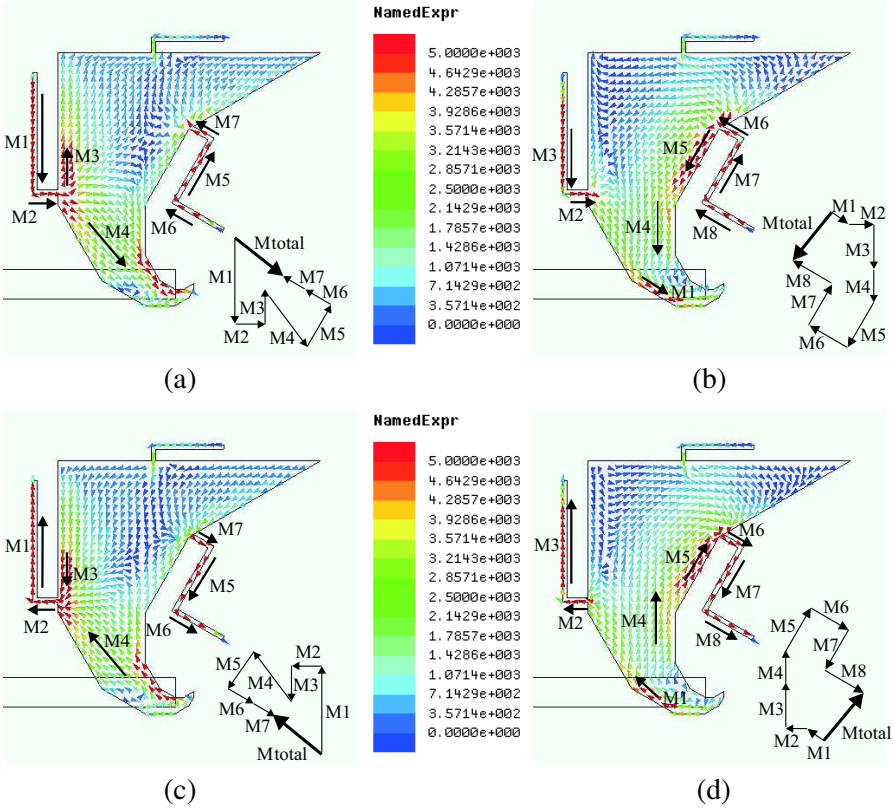

Figure 5. Simulated magnetic current distribution with period T at 3.1 GHz: (a) $t = 0$, (b) $t = T/4$, (c) $t = 2T/4$, and (d) $t = 3T/4$.

Spidron fractal slot rise and their vector sum points from the upper left corner to the lower right corner. At $t = T/4$, the currents near slits $S1$ and $S2$ and the Spidron fractal slot dominate the radiation again, producing a vector sum pointing from the upper right corner to the lower left corner. This vector sum is orthogonal to that at $t = 0$ and rotates clockwise as the time t increases, thus producing CP radiation, as shown in Fig. 5. As shown in Fig. 6, it was found that the currents on the Spidron fractal slot are the major components related to the generation of CP radiation at 4.2 GHz. Fig. 7 illustrates the current distribution at 5.0 GHz. Unlike the cases at 3.1 GHz and 4.2 GHz, this figure shows that slit $S3$ is involved in the current generation, rotating clockwise.

In the proposed antenna design, a conducting reflector is also applied to reduce back radiation from the Spidron fractal slot and

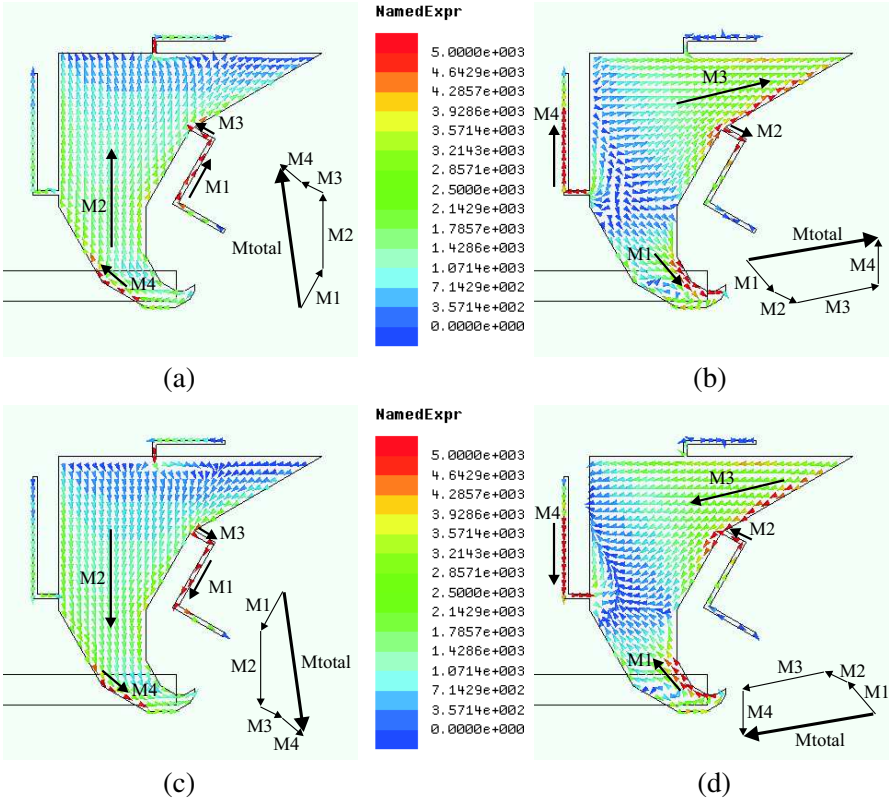

Figure 6. Simulated magnetic current distribution with period T at 4.2 GHz: (a) $t = 0$, (b) $t = T/4$, (c) $t = 2T/4$, and (d) $t = 3T/4$.

slits. Fig. 8 shows the effect of the reflector on forward antenna gain. By using the reflector, the peak gain of the antenna is significantly increased due to the suppression of back radiation. On the basis of the parametric study, the optimized parameters of the proposed antenna are derived and listed in the caption of Fig. 2.

4. EXPERIMENTAL RESULTS AND DISCUSSION

Based on the optimized parameters, the proposed antenna was fabricated and measured. Fig. 9(a) shows a photograph of the fabricated antenna. The Spidron fractal slot and three slits were etched from the top conducting layer of the substrate. The 50 Ω microstrip line was mounted on the bottom layer of the substrate. The reflector

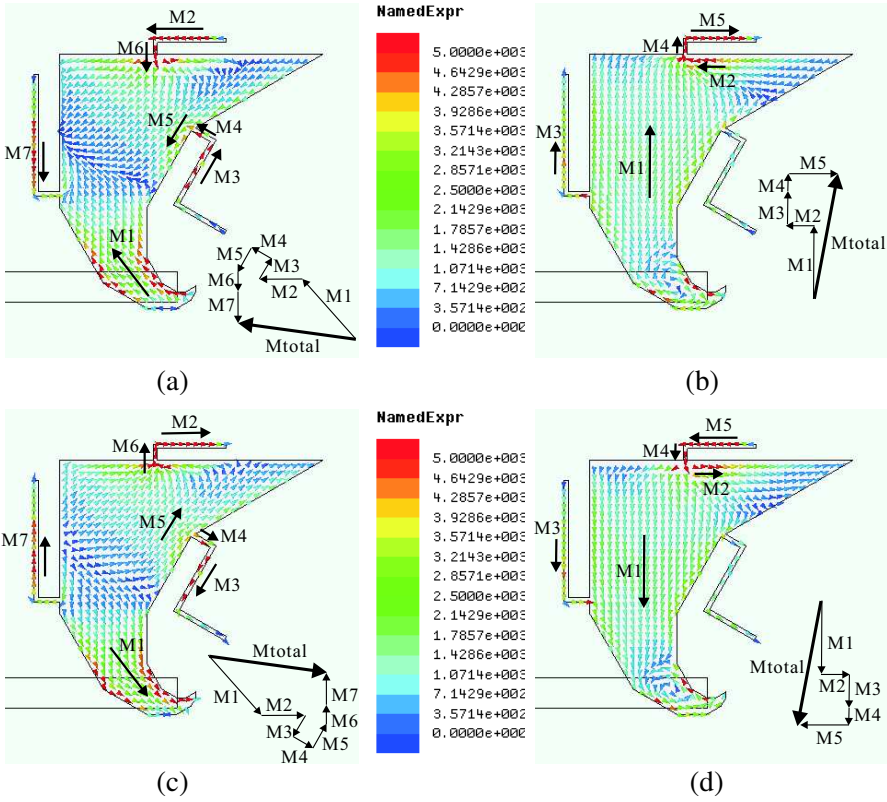

Figure 7. Simulated magnetic current distribution with period T at 5.0 GHz: (a) $t = 0$, (b) $t = T/4$, (c) $t = 2T/4$, and (d) $t = 3T/4$.

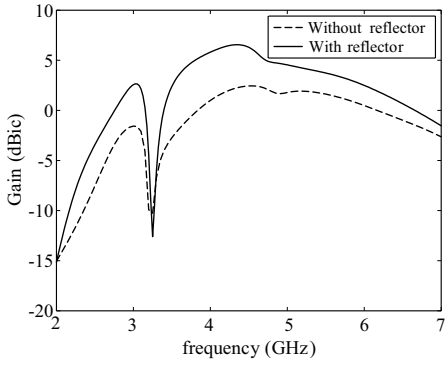

Figure 8. Simulated peak gains versus frequency in case of with and without a conducting reflector.

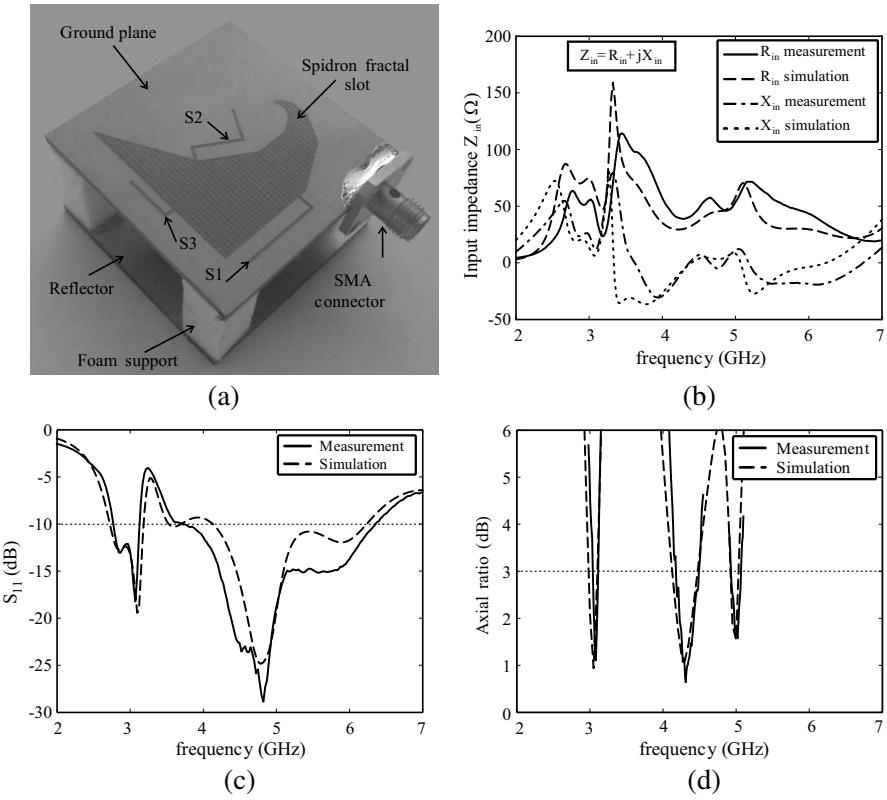

Figure 9. (a) Photograph of the fabricated antenna and simulated and measured (b) input impedances, (c) reflection coefficients, and (d) axial ratios of the proposed antenna.

was located at a distance of 17 mm under the bottom layer of substrate. Four foam supports with a relative permittivity of 1.06 were utilized to support the substrate, which was suspended in midair above the reflector. An Agilent 8510C network analyzer was used to measure the reflection coefficient of the proposed antenna. Figs. 9(b) and 9(c) show the simulated and measured input impedances and reflection coefficients, respectively. The measured −10 dB reflection coefficient bandwidths are from 2.76 GHz to 3.13 GHz and from 3.56 GHz to 6.22 GHz. The slight discrepancy between the simulation and the measurement can be attributed to the fabrication tolerance. The simulated and measured ARs in the broadside direction ($\theta = 0^\circ$) are shown in Fig. 9(d). It is noted that the measured result agrees well with the simulated result. The measured 3 dB AR bandwidths are 2.28%

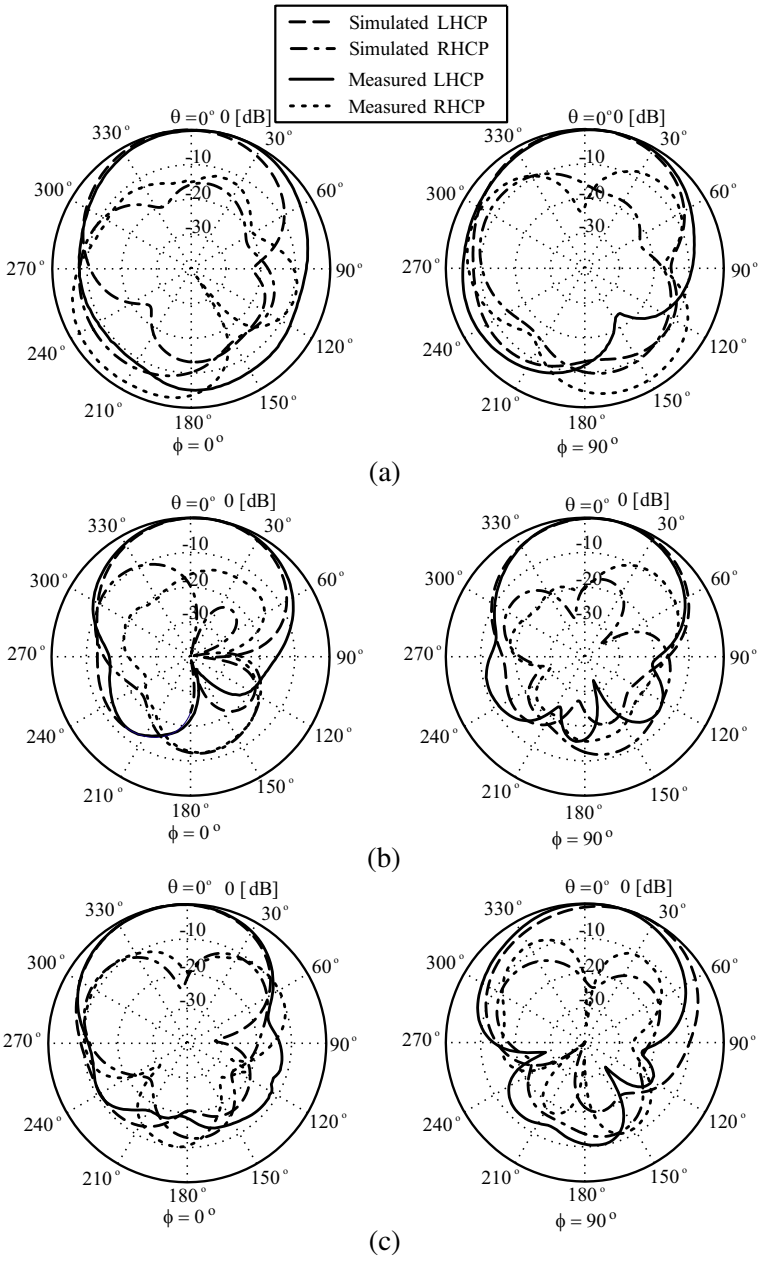

Figure 10. Simulated and measured normalized radiation patterns of the proposed antenna at operating CP frequencies: (a) 3.1 GHz, (b) 4.2 GHz, and (c) 5.0 GHz.

(3.04–3.11 GHz) for the lower band, 7.15% (4.18–4.49 GHz) for the middle band, and 2.6% (4.93–5.06 GHz) for the upper band. Table 1 shows a comparison of the 3 dB AR bandwidths for all operating bands of the proposed antenna, alongside antennas presented in earlier works [16, 17, 19, 20]. As shown in the table, the 3 dB AR bandwidths of the proposed antenna are wider than those of the previous triple-band CP antennas. Fig. 10 illustrates the simulated and measured normalized radiation patterns of the proposed antenna along two elevation cuts (xz- and yz-planes) at three frequencies. It is seen that the radiation patterns are directional to the positive z-axis due to the presence of the conducting reflector. Moreover, in both planes,

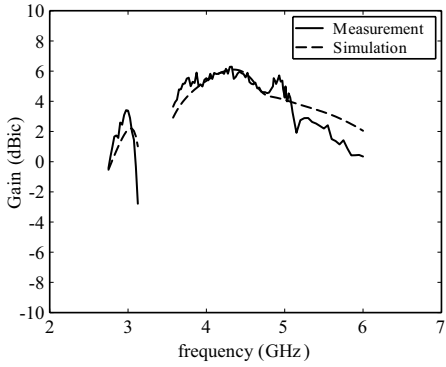

Figure 11. Simulated and measured peak gains of the proposed antenna.

Table 1. Comparison of the AR bandwidths between the proposed antenna and other triple-band CP antennas.

Structure	Lower band	Middle band	Upper band
Proposed antenna	3.04–3.11 GHz (2.28%)	4.18–4.49 GHz (7.15%)	4.93–5.06 GHz (2.6%)
[16]	1.156–1.196 GHz (3.4%)	1.222–1.232 GHz (0.81%)	1.569–1.582 GHz (0.83%)
[17]	1.567–1.577 GHz (0.64%)	1.596–1.611 GHz (0.93%)	2.486–2.502 GHz (0.64%)
[19]	1.485–1.515 GHz (2.0%)	2.48–2.52 GHz (1.6%)	4.875–4.925 GHz (1.02%)
[20]	1.518–1.583 GHz (4.19%)	2.375–2.46 GHz (3.52%)	2.985–3.015 GHz (1.0%)

the co-polarization (left-hand circular polarization, or LHCP) to cross-polarization (right-hand circular polarization, or RHCP) level is more than 15.7 dB in the broadside direction at all frequencies. Fig. 11 shows the simulated and measured LHCP gains of the proposed antenna. As seen in the figure, the peak gains within −10 dB reflection coefficient bandwidths are 3.41 dBic and 6.29 dBic, respectively.

5. CONCLUSION

A single microstrip-fed Spidron fractal slot antenna with three slits was proposed and studied for triple-band CP applications. By utilizing a Spidron fractal slot, a Z-shaped slit, and two L-shaped slits, triple-band CP radiation was realized. The parametric analysis proved that the proposed antenna had not only wide bandwidth but also independent tuning capability for three operating frequencies. The optimized antenna, fabricated on a commercial substrate, also exhibited directional radiation patterns for the entire measured frequencies. Therefore, the proposed CP antenna can be feasibly applied in various multi-band wireless communication systems.

ACKNOWLEDGMENT

This work was supported by Basic Science Research Program through the National Research Foundation of Korea (NRF) funded by the Ministry of Education, Science and Technology (2012R1A1A1038849).

REFERENCES

1. Rao, P. N. and N. V. S. N. Sarma, "Fractal boundary circularly polarised single feed microstrip antenna," *Electron. Lett.*, Vol. 44, No. 12, 713–714, 2008.
2. Zarifi, D., H. Oraizi, and M. Soleimani, "Improved performance of circularly polarized antenna using semi-planar chiral metamaterial covers," *Progress In Electromagnetics Research*, Vol. 123, 337–354, 2012.
3. Segovia-Vargas, D., F. J. Herraiz-Martinez, E. Ugarte-Munoz, L. E. Garcia-Munoz, and V. Gonzalez-Posadas, "Quad-frequency linearly-polarized and dual-frequency circularly-polarized microstrip patch antennas with CRLH loading," *Progress In Electromagnetics Research*, Vol. 133, 91–115, 2013.
4. Deng, J., L. Guo, T. Fan, Z. Wu, Y. Hu, and J. Yang, "Wideband circularly polarized suspended patch antenna with indented edge

and gap-coupled feed," *Progress In Electromagnetics Research*, Vol. 135, 151–159, 2013.

5. Wang, P., G. Wen, J. Li, Y. Huang, L. Yang, and Q. Zhang, "Wideband circularly polarized UHF RFID reader antenna with high gain and wide axial ratio beamwidths," *Progress In Electromagnetics Research*, Vol. 129, 365–385, 2012.
6. Meng, F.-Y., R.-Z. Liu, K. Zhang, D. Erni, Q. Wu, L. Sun, and L.-W. Li, "Automatic design of broadband gradient index metamaterial lens for gain enhancement of circularly polarized antennas," *Progress In Electromagnetics Research*, Vol. 141, 17–32, 2013.
7. Li, X., X. Ren, Y. Yin, L. Chen, and Z. Wang, "A wideband twin-diamond-shaped circularly polarized patch antenna with gap-coupled feed," *Progress In Electromagnetics Research*, Vol. 139, 15–24, 2013.
8. Lai, X.-Z., Z.-M. Xie, and X.-L. Cen, "Design of dual circularly polarized antenna with high isolation for RFID application," *Progress In Electromagnetics Research*, Vol. 139, 25–39, 2013.
9. Liu, W., Z. Zhang, and Z. Feng, "A bidirectional circularly polarized array of the same sense based on CRLH transmission line," *Progress In Electromagnetics Research*, Vol. 141, 537–552, 2013.
10. Lee, W.-S., K.-S. Oh, and J.-W. Yu, "A wideband circularly polarized pinwheel-shaped planar monopole antenna for wireless applications," *J. Electromagn. Eng. Sci.*, Vol. 12, No. 2, 155–160, 2012.
11. Ta, S. X., J. J. Han, and I. Park, "Compact circularly polarized composite cavity-backed crossed dipole for GPS applications," *J. Electromagn. Eng. Sci.*, Vol. 13, No. 1, 44–49, 2013.
12. Bao, X. L. and M. J. Ammann, "Dual-frequency circularly-polarized patch antenna with compact size and small frequency ratio," *IEEE Trans. on Antennas and Propag.*, Vol. 55, No. 7, 2104–2107, 2007.
13. Hsieh, G.-B., M.-H. Chen, and K.-L. Wong, "Single-feed dual-band circularly polarised microstrip antenna," *Electron. Lett.*, Vol. 34, No. 12, 1170–1171, 1998.
14. Jan, J.-Y. and K.-L. Wong, "A dual-band circularly polarized stacked elliptic microstrip antenna," *Microw. Opt. Technol. Lett.*, Vol. 24, No. 5, 354–357, 2000.
15. Sun, X., Z. Zhang, and Z. Feng, "Dual-band circularly polarized stacked annular-ring patch antenna for GPS application," *IEEE*

Antennas Wireless Propag. Lett., Vol. 10, 49–52, 2011.

16. Falade, O. P., M. U. Rehman, Y. Gao, X. Chen, and C. G. Parini, "Single feed stacked patch circular polarized antenna for triple band GPS receivers," *IEEE Trans. on Antennas and Propag.*, Vol. 60, No. 10, 4479–4484, 2012.
17. Liao, W., Q.-X. Chu, and S. Du, "Tri-band circularly polarized stacked microstrip antenna for GPS and CNSS applications," *Proc. 2010 International Conference on Microwave and Millimeter Wave Technology (ICMMT)*, 252–255, Chengdu, China, 2010.
18. Jinghui, Q., L. Hongmei, Y. Caitian, and L. Wei, "A triple-frequency circularly polarized microstrip patch antenna," *Proc. IEEE MTT-S Int. Microw. Symp. Dig.*, 190–193, San Francisco, United States, 2006.
19. Oraizi, H. and S. Hedayati, "Circularly polarized multiband microstrip antenna using the square and Giuseppe Peano fractals," *IEEE Trans. on Antennas and Propag.*, Vol. 60, No. 7, 3466–3470, 2012.
20. Wang, L., Y.-X. Guo, and W. X. Sheng, "A single-feed tri-band circularly polarized dual-annular slot antenna for wireless applications," *Journal of Electromagnetic Waves and Applications*, Vol. 26, Nos. 11–12, 1389–1396, 2012.
21. Fujimoto, T. and Y. Tagawa, "Triple band circularly polarized small microstrip antenna," *Proc. 2010 IEEE Antennas and Propagation Society International Symposium (APSURSI)*, 1–4, Toronto, Canada, 2010.
22. Karmakar, A., R. Ghatak, U. Banerjee, and D. R. Poddar, "An UWB antenna using modified Hilbert curve slot for dual band notch characteristics," *Journal of Electromagnetic Waves and Applications*, Vol. 27, No. 13, 1620–1631, 2013.
23. Karmakar, A., S. Verma, M. Pal, and R. Ghatak, "Planar fractal shaped compact monopole antenna for ultrawideband imaging systems," *International Journal of Microwave and Optical Technology*, Vol. 7, No. 4, 262–267, 2012.
24. Hwang, K. C., "Broadband circularly-polarised Spidron fractal slot antenna," *Electron. Lett.*, Vol. 45, No. 1, 3–4, 2009.
25. Trinh-Van, S., H. B. Kim, G. Kwon, and K. C. Hwang, "Circularly polarized Spidron fractal slot antenna arrays for broadband satellite communications in Ku-band," *Progress In Electromagnetics Research*, Vol. 137, 203–218, 2013.
26. "Ansoft high frequency structure simulator (HFSS)," Ver. 11. [Online]. Available: http://www.ansoft.com.